Applied Surface Science 527 (2020) 146908

Contents lists available at ScienceDirect

Applied Surface Science

journal homepage: www.elsevier.com/locate/apsusc

Simultaneous nitrogen doping and Cu_2O oxidization by one-step plasma treatment toward nitrogen-doped Cu_2O@CuO heterostructure: An efficient photocatalyst for H_2O_2 evolution under visible light

Wenwen Zhang[a], Xi Chen[b], Xiaoting Zhao[a], Mengyuan Yin[a], Luping Feng[b], Hua Wang[a,b,*]

[a] Institute of Medicine and Materials Applied Technologies, College of Chemistry and Chemical Engineering, Qufu Normal University, Qufu City, Shandong Province 273165, PR China

[b] School of Chemistry and Chemical Engineering, Harbin Institute of Technology, Harbin, Heilongjiang 150090, PR China

ARTICLE INFO

Keywords:
Plasma-assisted N doping
Cu_2O oxidization
Cu_2O@CuO heterostructure
Visible-light-driven photocatalysis
H_2O_2 production

ABSTRACT

An efficient photocatalyst of nitrogen (N)-doped Cu_2O@CuO was constructed for H_2O_2 production under visible light simply by the one-step N_2 plasma treatment for Cu_2O octahedrons. It was discovered that the plasma treatment could allow for the simultaneous N doping and Cu_2O oxidation to yield the N-doped Cu_2O@CuO heterostructure so as to boost the separation and transferring of photogenerated carriers of photocatalysis. More interestingly, the photocatalytic performances of the N-doped Cu_2O@CuO could controllably depend on the plasma treatment time, with the highest H_2O_2 production rate (about 14 $\mu Mg^{-1}min^{-1}$) at the 10-min plasma treatment, which is over three and eight folds higher than that of Cu_2O and CuO, respectively. Also, high photochemical stability of the photocatalyst could be expected for photocatalytic cycles. A two-step single electron transfer pathway was demonstrated for the photocatalytic oxygen reduction reactions of H_2O_2 evolution through the formation of dominated $^{\cdot}O_2^-$ radicals. This one-step plasma treatment route may provide a facile and efficient construction of photocatalytic heterostructures, promising for the large-scale applications for designing various efficient photocatalysts for H_2O_2 productions under visible light.

1. Introduction

Hydrogen peroxide (H_2O_2) as an effective green oxidant has drawn much attention in the fields of biological process, environmental remediation, and water purification [1–3]. At present, many classic technologies for producing H_2O_2 have been developed such as the electrochemical synthesis, anthraquinone autoxidation, and alcohols oxidation [4–6]. However, most of these approaches may have been trapped by some limitations like energy consumption, impurity introduction and explosion risk [7,8]. Therefore, developing a facile, safe, environmentally friendly, and energy-efficient method for H_2O_2 production is highly desired.

In recent years, increasing efforts have been focused on the development of photocatalytic H_2O_2 production technologies especially those featuring the merits of solar-driving, energy-saving, and green process [9–11]. In general, the efficiencies of the photocatalytic H_2O_2 generations may be largely depend on the functional performances of photocatalysts. Among various photocatalysts, cuprous oxide (Cu_2O) semiconductor, one of the cost-effectiveness, earth-abundance, and low-toxicity photocatalysts with a short bandgap (about 2.17 eV), can facilitate the photocatalysis applications in many fields typically as the photocatalytic water splitting for H_2/O_2 evolution and photodecomposition of organic pollutants [12–16]. However, some intrinsic disadvantages of Cu_2O such as the short hole-diffusion length and easy photochemical corrosion, may challenge the photocatalytic efficiency and stability, which may limit its photocatalytic applications on a large scale [17,18]. Aiming to solve these current problems, many researchers have tried to design Cu_2O-derivatized nanocomposites with improved photocatalytic activities by adjusting the facets, sizes, and morphologies of photocatalysts [19–21]. For example, Liu and coworkers created Cu_2O@TiO_2 photocatalysts with exposed Cu_2O facets for the efficient photocatalytic degradation of methylene blue and 4-nitrophenol under visible light [19]. Catherine et al. utilized amino acids to tune the size and morphology of Cu_2O achieving enhanced

* Corresponding author at: Institute of Medicine and Materials Applied Technologies, College of Chemistry and Chemical Engineering, Qufu Normal University, Qufu City, Shandong Province 273165, PR China.
E-mail address: huawang@qfnu.edu.cn (H. Wang).
URL: http://wang.qfnu.edu.cn (H. Wang).

https://doi.org/10.1016/j.apsusc.2020.146908
Received 12 March 2020; Received in revised form 1 June 2020; Accepted 2 June 2020
Available online 06 June 2020

photocatalysis for the degradation of methyl orange [21]. Moreover, it is well recognized that the doping of various heteroatoms such as nitrogen (N), phosphorus, and carbon can increase the active sites of photocatalysts with improved photocatalytic activities [22–25]. For example, Dubale and colleagues have fabricated an efficient photocatalyst by doping phosphorus into carbon/Cu_2O composites toward efficient photocatalytic phenol degradation and hydrogen production [22]. In particular, the construction of heterostructures has attracted extensive interests in improving the photocatalytic performances of Cu_2O-based photocatalysts [26–28]. For example, Li's group fabricated CuO/Cu_2O heterostructures with better photocatalytic activities for photo-degrading organic dyes [26]. Kim et al. developed $BiVO_4$/C/Cu_2O nanocomposites with Z-scheme-based heterostructures showing the promoted electron-hole separation for the increased photocatalysis for CO_2 reduction [28]. However, either the current heteroatoms doping methods or the heterostructures construction routes might mostly be challenged by some shortcomings like time-consuming process, complex operation, and harsh reaction conditions (i.e., high temperature and pressure). Therefore, it is of essential interest to develop a rapid, simple, and controllable strategy for the simultaneous Cu_2O-based heterostructures construction and heteroatoms doping to realize the efficient photocatalysis for H_2O_2 production under visible light.

Up to date, the plasma treatment technology as a facile, rapid, and efficient route has been widely utilized for the construction or surface modification of functional materials without the use of any solvent [29–31]. For example, Zhang and coworkers described the rapid synthesis of CoN nanowires by the N_2 plasma treatment of Co_3O_4 nanowires for oxygen evolution [29]. Wang's group employed the N_2 plasma for doping nitrogen into CoFe nanosheets for the enhanced electrocatalytic water oxidation [30]. Also, they employed Ar plasma to engrave Co_3O_4 nanosheets to create the reactive oxygen vacancies as well as enhanced specific surface area towards the improved electrocatalysis [31].

In the present work, an efficient photocatalyst with N-doped Cu_2O@CuO heterostructure has been constructed controllably by the one-step N_2 plasma treatment route for H_2O_2 production under visible light. Octahedral Cu_2O was first synthesized by the glucose reduction and then treated by the N_2 plasma, achieving the simultaneous Cu_2O oxidation and N doping. The resulted photocatalyst with N-doped Cu_2O@CuO heterostructure could achieved the greatly increased visible-light absorption and separation of photogenerated carriers, in which the introduced N heteroatoms and CuO in Cu_2O octahedron might serve as the photogenerated electron acceptor and electron donor, respectively. The enhanced photocatalysis performances of N-doped Cu_2O@CuO photocatalyst were thus obtained controllably depending on the plasma treatment time, as evidenced in the photocatalytic reduction of O_2 in water towards H_2O_2 production under visible light. The possible photocatalytic mechanism of two-step single electron pathway for the O_2 reduction was further explored by the capture experiments for active species. To the best of our knowledge, this is the first report on the simultaneous heteroatoms (i.e., N) doping and metal oxidation by the one-step N_2 plasma treatment towards the construction of the heterostructures for the efficiently photocatalytic H_2O_2 production under visible light.

2. Experimental section

2.1. Materials and Reagents.

Copric chloride dihydrate ($CuCl_2{\cdot}2H_2O$, 99.0%), glucose ($C_6H_{12}O_6$, 98.5%), isopropanol (IPA), and benzoquinone (BQ) were purchased from Sinopharm Chemical Reagent Co. Ltd. (Shanghai, China). p-hydroxyphenylacetic acid (PHPAA) was obtained from Sigma-Aldrich Co. Ltd. (Shanghai, China). Potassium hydrogen phthalate (PHP) and horseradish peroxidase (HRP) were bought from Sangon Biotech Co., Ltd. (Shanghai, China). Other chemicals are of analytical grade. Deionized water (> 18.2 Mohm-cm) was provided by ultra-pure water system (Pall, USA).

2.2. Synthesis of photocatalytic Materials.

2.2.1. Synthesis of CuO

An aliquot of 0.0394 g $CuCl_2{\cdot}2H_2O$ was used as copper source to be dissolved into 46.2 mL water. Following that, 13.8 mL ammonia solution (0.90 g·mL^{-1}) was dropped into $CuCl_2$ solution to be stirred for 10 min. Then, the mixture was adjusted to pH 12 by NaOH (0.40 g mL^{-1}) and further stirred for 20 min. Afterwards, the as-prepared mixture was transferred into 50 mL Teflon-lined autoclave to be heated at 160 °C for 8 h, and then cooled down to room temperature. Subsequently, after being centrifuged and washed with water and ethanol, the so obtained products of CuO were dried at 60 °C overnight and finally stored in dark.

2.2.2. Synthesis of N-doped Cu_2O@CuO

The N-doped Cu_2O@CuO composites were synthesized by the N_2 plasma treatment of Cu_2O octahedrons. Herein, Cu_2O was first fabricated by following the procedure. Typically, an aliquot of 0.0394 g $CuCl_2{\cdot}2H_2O$ was dissolved into 46.2 mL water, followed by the introduction of 3.8 mL ammonia solution (0.90 g·mL^{-1}). After the mixture was first adjusted to pH 12 by NaOH (0.4 g·mL^{-1}) and then stirred for 20 min, 15 mL $C_6H_{12}O_6$ (3.05 mg·mL^{-1}) was introduced into the mixture (40 mL) to be further stirred for 10 min. Then, the mixture was incubated at 60 °C for 30 min to be centrifuged and washed separately with water and ethanol. After that, the obtained products of octahedral Cu_2O were dried at 60 °C overnight. Moreover, the so prepared octahedral Cu_2O powder was spread on the quartz boat in the plasma chamber (RF 13.56 MHz, 45 W), into which N_2 was introduced at a flowing rate of 50 sccm under the pressure of 100 Pa, to be treated for different times of 5.0, 10, and 15 min. Subsequently, the resulted N-doped Cu2O@CuO products were stored in dark for future usage.

2.3. Characterization of photocatalytic materials

The crystal structures of photocatalysts were recorded on an X-ray diffraction (XRD, PANalytical/X pert3) with Cu Kα radiation. Morphological structures of the products were explored separately by field-emission scanning electron microscopies (SEM, Hitachi E-1010, Horiba Ex-250) and transmission electron microscopy (TEM, JEOL/JEM-2100PLUS). Moreover, the UV–vis spectra of the different materials were measured by UV–vis spectrometer (Shimadzu UV-3600, Japan) with $BaSO_4$ as the reference substance. Also, the chemical composition of photocatalysts were analyzed by Fourier transform infrared spectroscopy (Thermo Nicolet Nexus 470FT, USA) with KBr as the reference substance. The amounts of hydrogen peroxide (H_2O_2) yielded in pure water were measured through monitoring the fluorescent products of the HRP-catalyzed H_2O_2-PHPAA reactions by using the fluorescence spectrometer (Horiba, FluoroMax-4, Japan). Besides, their electrochemical impedance spectra (EIS) and photocurrent responses were measured by the electrochemical work station (CHI 760D, Shanghai, China), in which a three-electrode system was utilized consisting of a platinum electrode as the working electrode, a saturated calomel electrode (SCE) as the reference, and a platinum wire electrode as the counter one.

Furthermore, the Mott-Schottky (M − S) plotting was performed to evaluate the flat band potentials of the photocatalytic materials, on the basis of the data of electrochemical measurements operated at an amplitude of 5.0 mV and a frequency of 1.0 kHz.

2.4. Photocatalytic applications of N-doped Cu_2O@CuO for H_2O_2 Production.

2.4.1. Photocatalytic H_2O_2 production experiments

The photocatalytic applications for H_2O_2 evolution were carried out by using a glass reactor and 300 W Xe-lamp (Yirida Technology Co. Ltd., Shenyang, China) with a 420 nm cut-off filter as the simulated sunlight source. Typically, an aliquot of 15 mg photocatalysts was dispersed into 10 mL H_2O to be stirred for one hour in dark to reach the equilibrium of adsorption and desorption. Afterwards, 500 μL of the suspension was collected for every 15 min and then centrifuged. Subsequently, 300 μL of the supernatant was fetched, in which the concentrations of H_2O_2 so produced were detected by the PHPAA-based analysis method reported previously [32]. Typically, an aliquot of 1.0 mL of fluorescence reagent (270 mg/L PHPAA, 30 mg/L HRP, and 8.2 g/L PHP) was separately introduced into the above supernatants to react for 2.0 h. Herein, HRP would catalyze the reactions between PHPAA and H_2O_2 so produced to form the fluorescent dimers in the PHP buffer. After that, 1.0 mL NaOH (1.0 M) was added to be mixed for 10 min. The fluorescence intensities of the products were finally measured using the fluorescence spectrophotometer at an excitation wavelength of 315 nm, by which the H_2O_2 concentrations were calculated.

2.4.2. Reactive species trapping experiments

To investigate the active reactive species possibly yielded in the process of N-doped Cu_2O@CuO photocatalysis, the trapping experiments for reactive species were performed with IPA (1.0 mM) and BQ (1.0 mM) serving as hydroxyl radicals scavenger and superoxide radicals scavenger, respectively. According to the same procedure of photocatalytic reactions of H_2O_2 production above, the reaction system was conducted under the visible-light irradiation using 300 W Xe-lamp.

3. Results and discussion

3.1. Fabrication and morphological analysis of photocatalytic materials

The N-doped Cu_2O@CuO photocatalysts were synthesized from Cu_2O octahedrons simply by a one-step N_2 plasma treatment, with the main fabrication procedure schematically illustrated in Scheme 1. Herein, Cu_2O octahedrons were firstly prepared by glucose reduction under the alkaline condition, and then treated by N_2 plasma to yield the N-doped Cu_2O@CuO nanocomposites. Fig. 1a, b manifest the comparison of the morphologies among Cu_2O octahedrons and N-doped Cu_2O@CuO nanocomposites by the scanning electron microscopy (SEM) imaging. One can note from Fig. 1a that pristine Cu_2O could present the regular octahedral structure with smooth surface showing the average size of about 600 nm in diameter. After the N_2 plasma treatment to produce N-doped Cu_2O@CuO, "small wings"-like paraphytes could be produced on the surface of Cu_2O octahedrons (Fig. 1b). To make a further insight of the resulted N-doped Cu_2O@CuO nanocomposites, the element mapping analysis was performed by energy dispersive spectroscopy (EDS), showing the Cu, O, N elements uniformly distributed (Fig. 1c). Fig. 2a–d display the transmission electron microscopy (TEM) images of N-doped Cu_2O@CuO, showing the "small wings"-like profile as more clearly revealed in the amplified view (Fig. 2b), which is well consistent with the ones in Fig. 1b above. Especially, a lattice analysis was further conducted for the selected areas of the amplified N-doped Cu_2O@CuO particle (Fig. 2c, d). As expected, one can note from Fig. 2c that the lattices measured from Cu_2O area could illustrate the average spacing of 0.24 nm, which can correspond to the (1 1 1) lattice facet of octahedral Cu_2O, as described elsewhere [20]. Besides, Fig. 2d reveals that the lattices measured from the surface "small wings" part of N-doped Cu_2O@CuO could have an average spacing of 0.23 nm, which may belong to the (1 1 1) lattice plane of CuO [26]. The data indicate that N-doped Cu_2O@CuO heterostructures could be constructed by the one-step plasma treatment for simultaneous N doping and Cu_2O oxidation.

3.2. Investigations on the structural and elemental composition

The XRD characterizations were first conducted to investigate the crystal structure of N-doped Cu_2O@CuO yielded by the N_2 plasma treatments for different time (5.0, 10, and 15 min), taking Cu_2O as the control (Fig. 3). One can note that the identified diffraction peaks located at 29.5°, 36.4°, 42.2°, 61.3°, 73.4°, and 77.3° can be assigned to (1 1 0), (1 1 1), (2 0 0), (2 2 0), (3 1 1), and (2 2 2) of Cu_2O (JCPDS 05-0667),[19] respectively. However, the diffraction peaks of CuO phase were not found in the XRD pattern of N-doped Cu_2O@CuO nanocomposites after being treated by N_2 plasma for 10 min, due to that the amount of CuO yielded on the surface of nanocomposites might be too low to be detected by the XRD. Moreover, the chemical states of different elements in N-doped Cu_2O@CuO nanocomposites were explored by X-ray photoelectron spectroscopy (XPS), taking pure Cu_2O as the control (Fig. 4). The wide-scan spectra indicate the existence of Cu, O and N elements in N-doped Cu_2O@CuO, in contrast to pure Cu_2O (Fig. 4a). By fitting the fine-scanned Cu 2p spectra, furthermore, the electronic states of Cu atoms with different valences were recognized with the data shown in Fig. 4b. As expected, the binding energies (BEs) at 932.17 eV and 952.00 eV could be observed corresponding to Cu 2p3/2 and Cu 2p1/2 of Cu (I), respectively, whereas the peaks located at 934.7 and 954.6 eV should be attributed to Cu^{2+} species formed on the surface of Cu_2O. Interestingly, two peaks of Cu^{2+} species might also be obtained for pure Cu_2O presumably due to the oxidation of a fraction of pure Cu_2O in air, which however are much lower than those in the N-doped Cu_2O@CuO. The results may confirm that CuO should be formed on the surface of Cu_2O after the N_2 plasma treatment [33]. Also, the ratio of CuO-to-Cu_2O was calculated to be about 0.10. Moreover, Fig. 4c manifests the high-resolution XPS spectra of O 1 s with the double peaks located at 530.35 eV and 531.5 eV, which can be assigned to the lattice oxygen and (e.g., O_2, hydroxyl species), respectively. Notably, the obvious decrease of surface-absorbed oxygen species of N-doped Cu_2O@CuO might indicate the part removal of surface oxygen after the

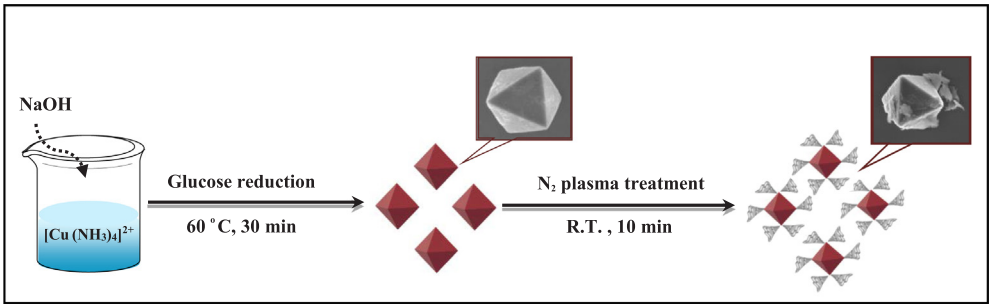

Scheme 1. Schematic illustration for the main fabrication procedure of N-doped Cu_2O@CuO photocatalysts by the N_2 plasma treatment route for Cu_2O octahedrons, showing the changing morphological structures of TEM images.

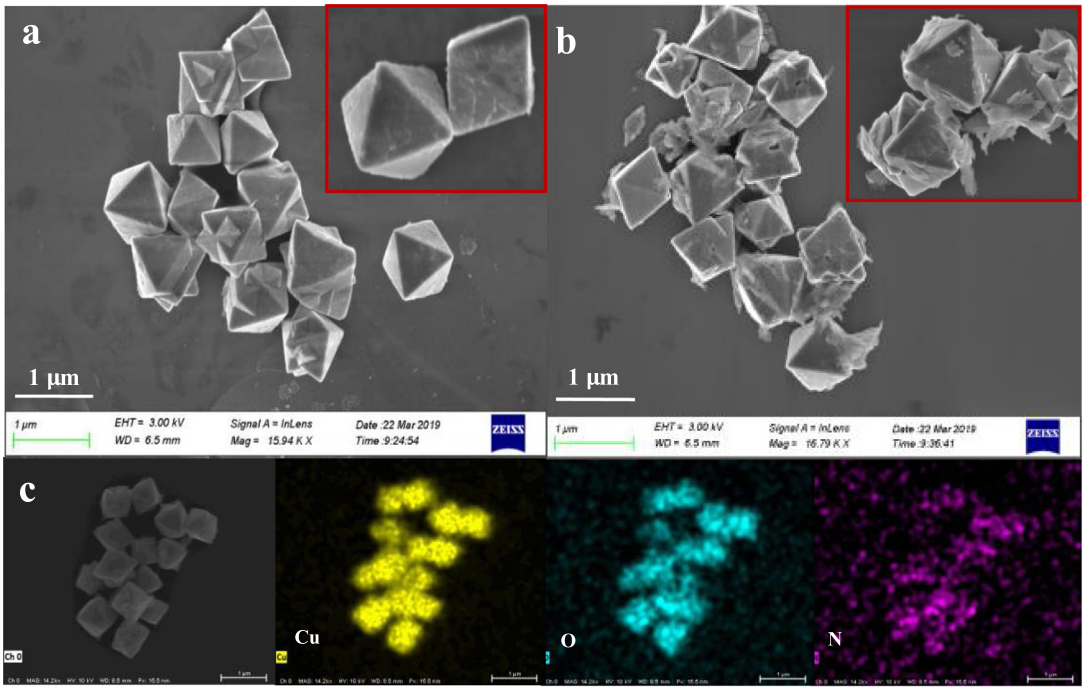

Fig. 1. SEM images of Cu_2O octahedrons (a) before and (b) after the 10-min N_2 plasma treatment to yield the N-doped Cu_2O@CuO nanocomposites with (c) the EDS element mapping of Cu, O, and N elements.

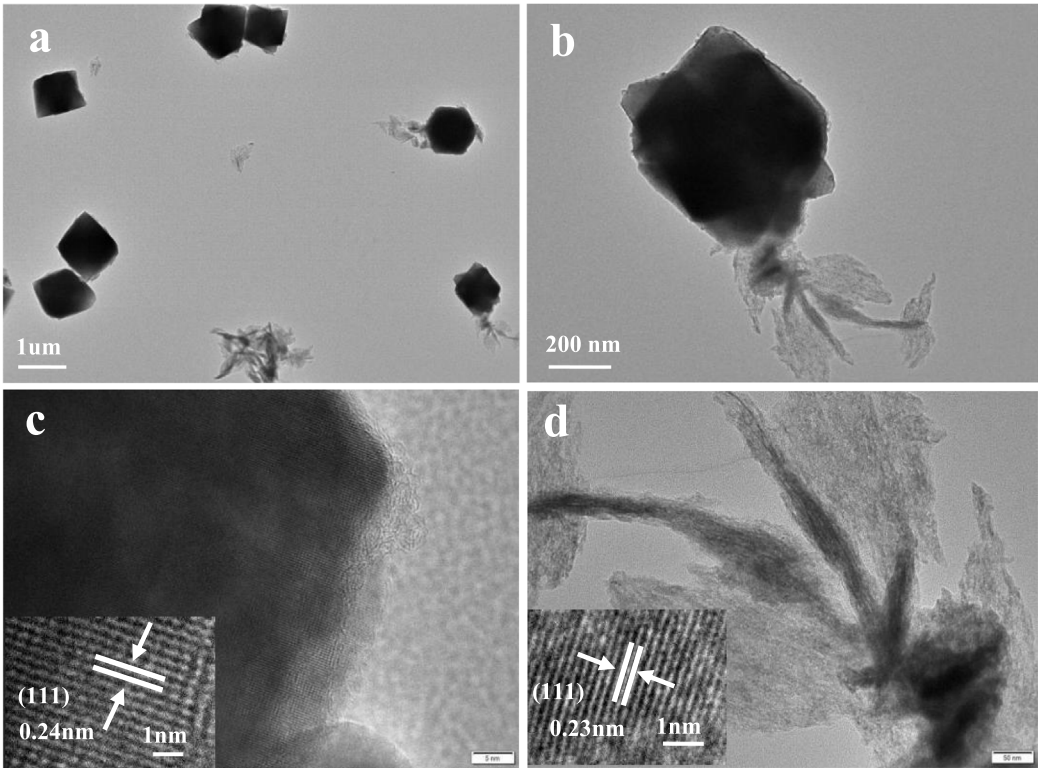

Fig. 2. TEM images of (a) N-doped Cu_2O@CuO nanocomposites yield by N_2 plasma treatment for Cu_2O octahedrons for 10 min, with (b–d) the amplified parts of a nanocomposites.

N_2 plasma treatment. What's more, the peak at 398.6 eV can be attributed to the Cu—N bond [34], indicating that N atoms were doped into Cu_2O (Fig. 4d). The results above indicate the successful fabrication of N-doped Cu_2O@CuO by the one-step N_2 plasma treatment for Cu_2O octahedrons.

3.3. Studies on the optical properties

To explore the light absorption abilities of the photocatalytic N-doped Cu_2O@CuO nanocomposites, their spectra of UV–Vis DRS were recorded in comparison with those of Cu_2O and CuO (Fig. 5a), of which the band gaps were calculated by the following formula: [35]

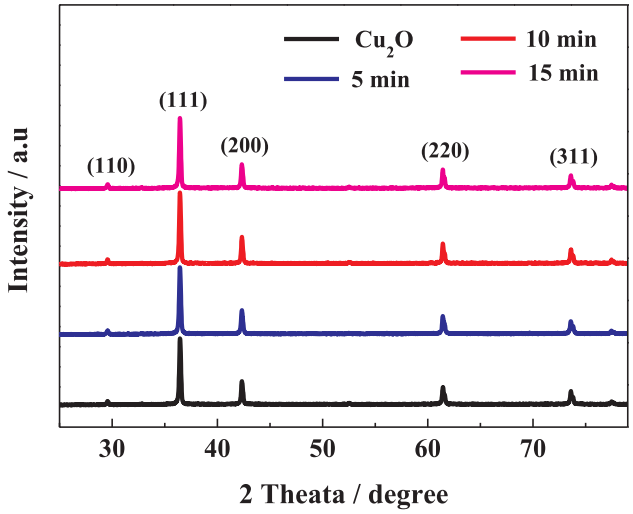

Fig. 3. XRD patterns of Cu_2O octahedrons before and after the nitrogen plasma treatment for different time of 5.0, 10, and 15 min to yield N-doped Cu_2O@CuO nanocomposites.

λg = 1239/Eg, where λg and Eg represent the observed optical absorption edge and the band gap, respectively. As can be seen from Fig. 5a, all of the tested materials could present the visible light responses, indicating that their light absorptions could occur because of the band transitions from the valence bands to the conduction ones. The band gap energies of 2.02 eV and 1.69 eV were thus calculated for Cu_2O and CuO, respectively, of which the absorption edges could separately correspond to 612 nm and 733 nm, suggesting that CuO might exhibit a broader optical harvest than Cu_2O. More importantly, the optical absorption edge of the developed N-doped Cu_2O@CuO could display a slight shift towards the higher wavelength (red shift) because of the formation of CuO. By compared with Cu_2O, therefore, a higher absorption could be achieved for the prepared N-doped Cu_2O@CuO nanocomposites, so as to afford a higher application efficiency of sunlight towards the improved photocatalytic activity. In order to further explore the functional groups of the developed photocatalysts, a comparison of FT-IR spectra was conducted between N-doped Cu_2O@CuO and pristine Cu_2O, with the data shown in Fig. 5b. Accordingly, Cu_2O showed the prominent peaks at 620 and 650 cm^{-1} corresponding to the Cu−O stretching vibrations [36]. Moreover, after the 10-min plasma treatment to yield the N-doped Cu_2O@CuO, the Cu−O stretching vibration peaks of Cu_2O could show a red shift, implying that the N element might be replaced by the O element. Nevertheless, there is no obvious Cu (II)-O vibration absorption peak, which might be ascribed to the relatively low content of CuO existing on the surface of Cu_2O. Conclusively, the N-doped Cu_2O@CuO could be successfully achieved by the one-step N_2 plasma treatment for Cu_2O octahedrons.

3.4. Photocatalytic performances and stability

The photocatalytic performances of the N-doped Cu_2O@CuO photocatalysts treated by N_2 plasma for different time were evaluated by comparing with pure Cu_2O and CuO, in which the H_2O_2 amounts produced from the O_2 reduction in pure water under visible light irradiation were monitored (Fig. 6a). One can see that all of the N-doped Cu_2O@CuO photocatalysts could attain much higher H_2O_2 yields. In contrast, the photocatalytic H_2O_2 productions for both pure Cu_2O and CuO are negligibly low, due to they might encounter with the fast recombination of photogenerated electron-hole pairs. Importantly, herein, the dramatically enhanced photocatalytic activity of N-doped Cu_2O@CuO heterostructure for photocatalytic H_2O_2 production might

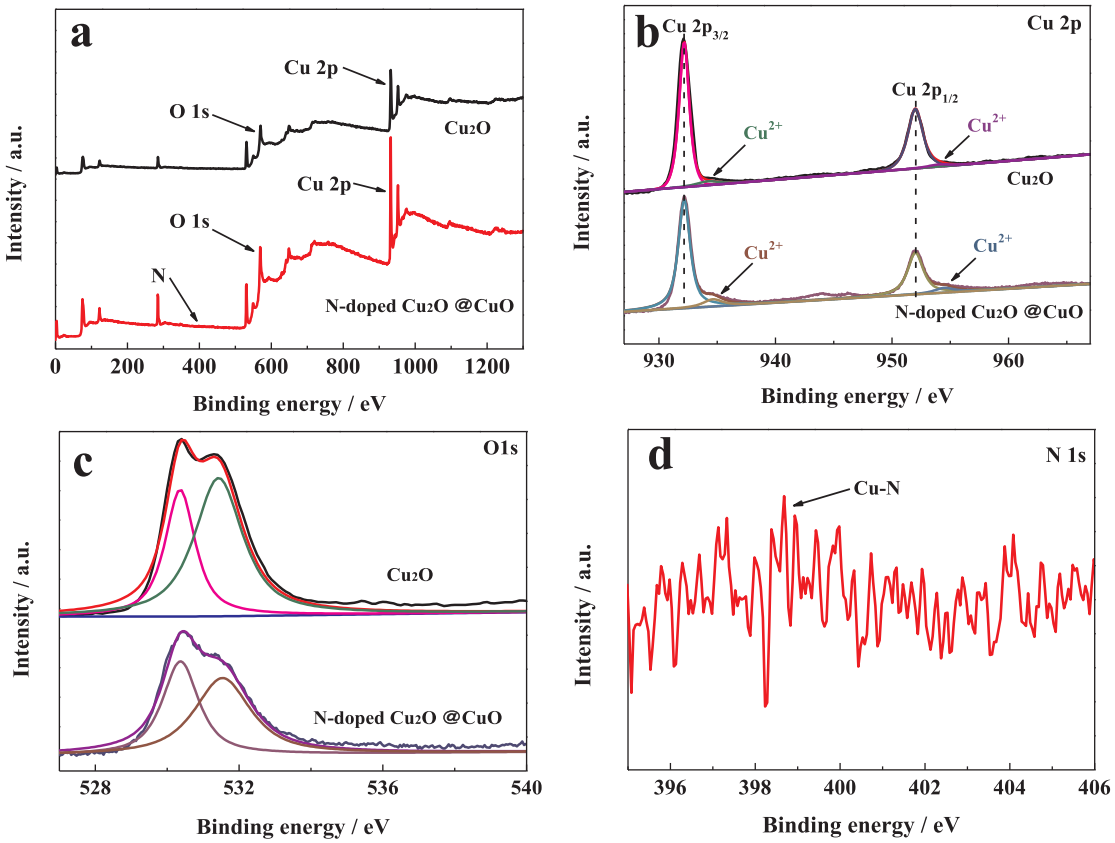

Fig. 4. XPS spectra of N-doped Cu_2O@CuO nanocomposites after the 10-min nitrogen plasma treatment of (a) full, (b) Cu 2p, (c) O 1s, and (d) N 1s, taking pure Cu_2O as the control.

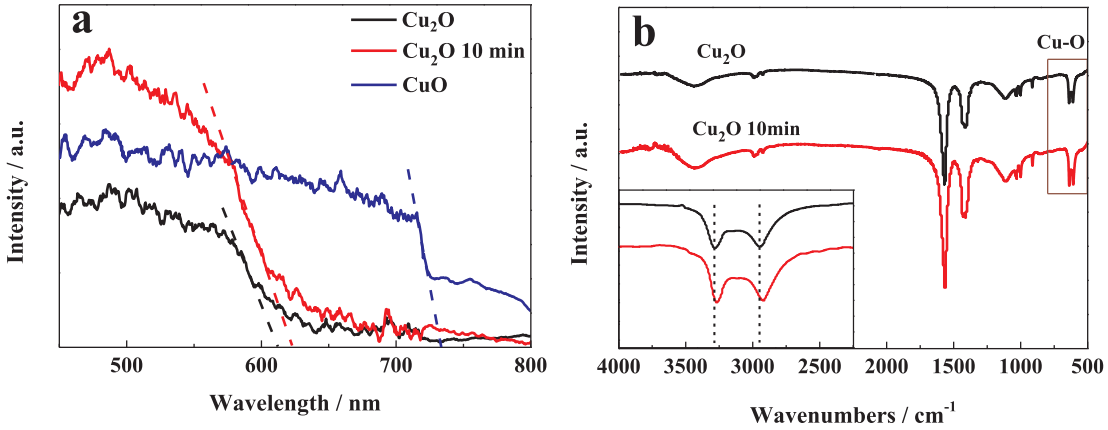

Fig. 5. (a) Comparable UV–vis and (b) FTIR spectra of CuO, Cu_2O octahedrons before (red) and after the 10-min N_2 plasma treatment to form N-doped Cu_2O@CuO nanocomposites (black). (For interpretation of the references to colour in this figure legend, the reader is referred to the web version of this article.)

be mainly attributed to the two facts. On the one hand, CuO derived on the surface of Cu_2O by the N_2 plasma-enabled in-situ oxidization might serve as a new active site for enriching more photogenerated electrons. On the other hand, the doped N might improve the charge separation ability of Cu_2O, thus facilitating the further increased photogenerated electrons of photocatalysts. More importantly, the highest photocatalytic H_2O_2 production could be achieved for the N-doped Cu_2O@CuO fabricated by 10-min N_2 plasma treatment with a H_2O_2 production of 12.6 μM after 60 min of visible light irradiation. Accordingly, the highest H_2O_2 production rate was calculated to be about 14 μM g^{-1} min^{-1}, which is over three and eight folds than those of pure Cu_2O and CuO, respectively (Fig. 6b). Therefore, the photocatalytic performances of N-doped Cu_2O@CuO photocatalysts can controllably depend on the treatment time of N_2 plasma, showing the best one formed by the N_2 plasma treatment time for 10 min. It indicates that the suitable treatment time of N_2 plasma might enhance photocatalytic activities of N-doped Cu_2O@CuO photocatalysts, presumably by improving the separation and transfer of photon-generated

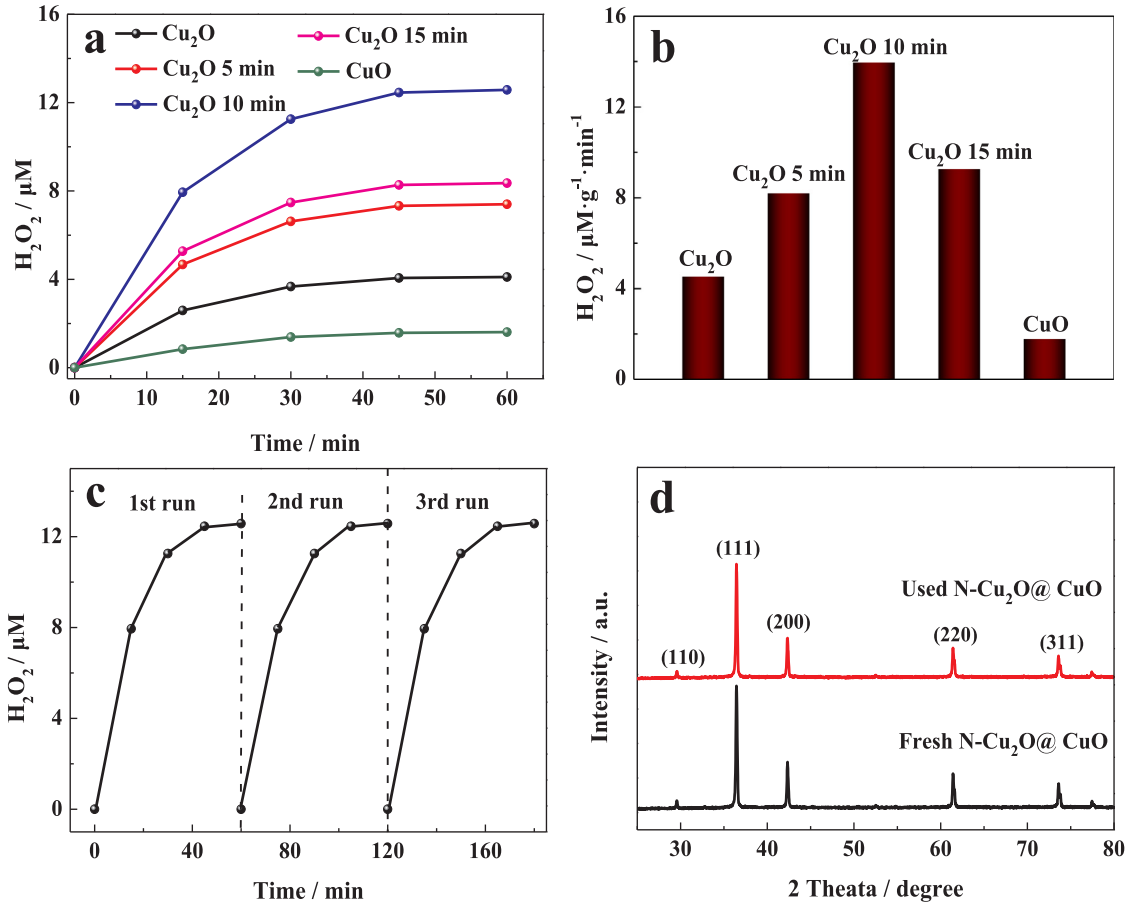

Fig. 6. (a) Time-dependent photocatalytic H_2O_2 yields and (b) rates of Cu_2O octahedrons and N-doped Cu_2O@CuO after the nitrogen plasma treatments for different time of 5.0–15 min, taking pristine CuO as the control. (c) Recycling experimental results of N-doped Cu_2O@CuO nanocomposites in the photocatalytic H_2O_2 generation reactions, and (d) XRD patterns of the nanocomposites before and after being used for three runs of photocatalytic reactions, where the nanocomposites were yielded by the 10-min N_2 plasma treatment for Cu_2O octahedrons.

carriers as demonstrated afterwards. However, too long plasma treatment time might bring about the excessive doping N, which might form the recombination centers of photogenic charge carriers in N-doped Cu_2O@CuO photocatalysts resulting in the inhibited photocatalytic activities [37].

The photochemical stability of the N-doped Cu_2O@CuO photocatalysts was further explored by the repeated experiments of photocatalytic H_2O_2 generations using the ones for 10-min treatment of N_2 plasma as example (Fig. 6c). One can observe that the developed photocatalyst could maintain a pretty high production of H_2O_2 after being reused for three cycles. Furthermore, the XRD patterns of N-doped Cu_2O@CuO were measured to characterize the recovered photocatalyst before and after the three-cycle reactions (Fig. 6d). It was found that the developed N-doped Cu_2O@CuO photocatalysts could exhibit no significant change in the phase structures after three-cycle usages for H_2O_2 productions, demonstrating the favorable photostability of photocatalysts.

3.5. Photocurrent reponses and electrochemical properties

The photogenerated charge separation as the premise of photocatalysis can be directly reflected by the transient photocurrent densities of photocatalysts [38–40]. In order to get further insight into the photogenerated charge transferring and carrier separation abilities, the transient photocurrents and electrochemical impedance spectra (EIS) were measured for the N-doped Cu_2O@CuO photocatalysts treated by N_2 plasma for different time by taking pure Cu_2O and CuO for comparison (Fig. 7). As expected in Fig. 7a, the largest photocurrent density could be obtained for the N-doped Cu_2O@CuO for the 10-min N_2 plasma treatment (1.0 μAcm^{-2}), which is about ten folds higher than that of pure Cu_2O. Importantly, such a transient photocurrent of N-doped Cu_2O@CuO could be switched reversibly and reproducibly by successive periodic illuminations, again showing the pretty high photocatalytic stability. Moreover, EIS measurements were conducted to estimate the kinetics of charge transferring among the photocatalysts in Fig. 7b. Herein, the Nyquist plots were fitted by a ZSimpWin software with the corresponding equivalent circuit model of Rs(QRct), containing the solution resistance (Rs), charge transfer resistance (Rct), and constant phase element (Q) between the modified electrode and electrolyte [41,42]. Clearly, the fitting solid lines might well match with the experimental results, demonstrating the feasibility of the selected equivalent circuit model. Furthermore, the fitted values of Rct were determined to be 336.5, 192, and 2764 for Cu_2O after being treated by N_2 plasma for 5 min, 10 min, and 15 min, respectively, in contrast to those of CuO (3606) and Cu_2O (551.3). Accordingly, the N-doped Cu_2O@CuO yielded by the 10-min N_2 plasma treatment should display the smallest Rct among the other photocatalytic materials, illustrating the fastest transferring rate of interface charge carriers. The data above indicate that the so developed photocatalysts could significantly improve the transferring rate and the separation efficiency of photogenerated electron-hole pairs, resulting in the efficient photocatalytic H_2O_2 production under visible light.

3.6. Possible photocatalytic pathway

To explore the transfer pathway of photogenerated carriers in the developed N-doped Cu_2O@CuO, the energy band structures of Cu_2O and CuO were first studied through the Mott-Schottky (MS) curves (Fig. 8a, b). The negative slopes of the MS plots confirm that the Cu_2O and CuO should be the p-type semiconductors. What's more, the flat band (FB) potentials of Cu_2O and CuO were obtained to be 1.28 and 1.50 V (vs Ag/AgCl), respectively. Further, the FB potentials versus the reversible hydrogen electrodes (RHE) could be calculated by the formula below ($E^{\ominus}_{AgCl}$ = 0.199 eV, pH 7.0):[40]

$$E_{fb\,(vs.\,RHE)} = E_{fb\,(vs.\,Ag/AgCl)} + 0.05916\,pH + E^{\ominus}_{Ag/AgCl}$$

$$E_{CB} = E_{VB} - Eg$$

where E_{CB} is the conduction band (CB) edge potential, E_{VB} represents the value band (VB) edge potential, and Eg is the band gap of the semiconductor. Therefore, $E_{fb\ (vs.\ RHE)}$ of Cu_2O and CuO was calculated to be about 1.88 and 2.11 eV, respectively. Considering that the E_{VB} of p-type semiconductors are generally approximate to the flat band potentials, the E_{VB} of Cu_2O and CuO were thus estimated to be 1.88 and 2.11 eV, respectively. Also, the CB potentials of Cu_2O and CuO were determined to be −0.14 and 0.42 V.

Moreover, it is well known that the photocatalyst may probably conduct double-channel reaction for H_2O_2 production relying on two types of active intermediates ($^{\cdot}O_2^-$ and $^{\cdot}OH$) [43,44]. Hence, the radical-trapping experiments were first performed to investigate the possible photocatalytic mechanism for the developed N-doped Cu_2O@CuO by using different scavengers of IPA and BQ, with the results shown in Fig. 8c. Obviously, the addition of IPA ($^{\cdot}OH$ scavenger) could exert no effect on the photocatalytic activity of N-doped Cu_2O@CuO, in contrast to BQ ($^{\cdot}O_2^-$ scavenger) that could conduct the apparent photocatalytic inhibition. Accordingly, $^{\cdot}O_2^-$ should be the main reactive species for the N-doped Cu_2O@CuO-photocatalyzed H_2O_2 production.

On the basis of the data above, the possible photocatalysis pathway of N-doped Cu_2O@CuO heterostructure is thus proposed by featuring a

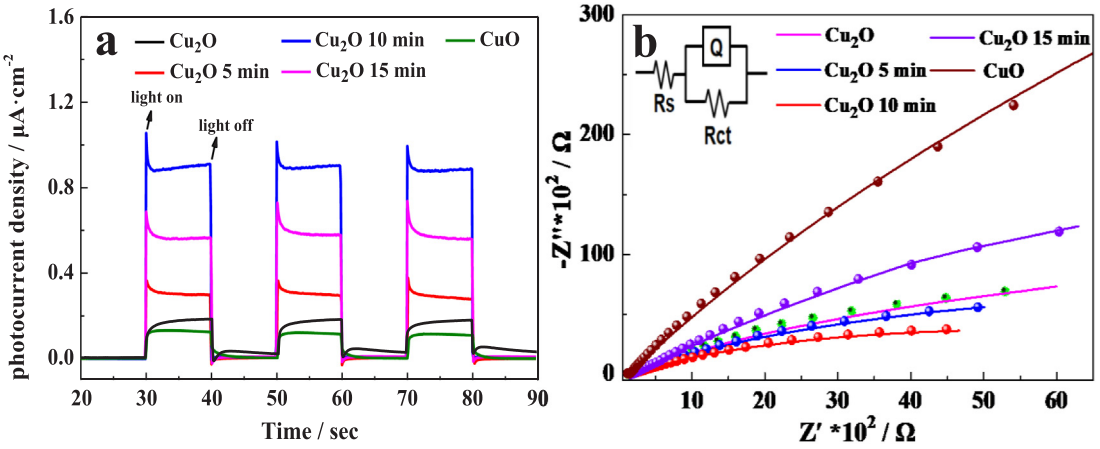

Fig. 7. (a) Comparable photocurrent responses under visible light irradiation, and (b) electrochemical impedance spectroscopy (EIS) of Cu_2O octahedrons before and after the nitrogen plasma treatment for different time of 5.0, 10, and 15 min to yield N-doped Cu_2O@CuO nanocomposites, taking pristine CuO as the control. The solid lines of Nyquist plotting were fitted by the ZSimpWin software with the corresponding equivalent circuit model (inset).

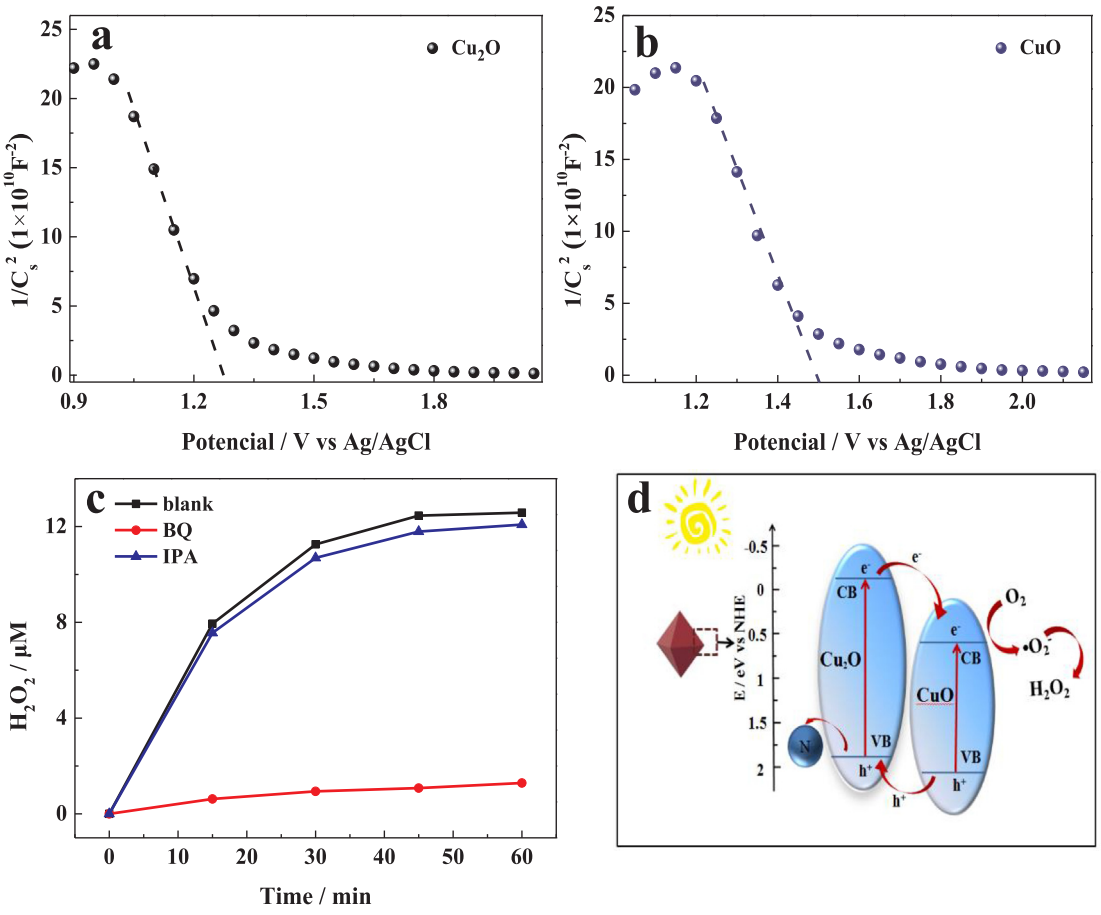

Fig. 8. (a-b) Mott-Schottky plots of Cu_2O octahedrons and CuO. (c) Reactive species-trapping experimental results using benzoquinone (BQ) and isopropanol (IPA) as the superoxide radicals ($^{\cdot}O_2^-$) and hydroxyl radicals ($^{\cdot}OH$) scavengers, respectively. (d) Schematic illustration of the photocatalytic mechanism underlying the photoexcited dynamics of N-doped Cu_2O@CuO nanocomposites in the photocatalytic H_2O_2 evolution reactions.

two-step single electron transfer ($O_2 \rightarrow {}^{\cdot}O_2^- \rightarrow H_2O_2$), as schematically illustrated in Fig. 8d. Considering that the CB and VB of Cu_2O are more negative than those of CuO, herein, once the N-doped Cu_2O@CuO was exposed to visible light, the activated electrons (e^-) might transfer from Cu_2O to CuO. Meanwhile, the holes (h^+) would transfer from CuO to Cu_2O. On one hand, the holes on the VB of Cu_2O might be captured by the doped N, resulting in the efficient separation photogenerated carriers of the developed photocatalyst. One the other hand, the photogenerated electrons of the photocatalysts might restore the dissolved oxygen into $^{\cdot}O_2^-$, which might be further turned into H_2O_2 via a two-step single electron transfer in the oxygen reduction reactions, due to the CB potential of CuO is more negative than those of $O_2/{}^{\cdot}O_2^-$ and $^{\cdot}O_2^-/H_2O_2$. The N-doped Cu_2O@CuO-photocatalyzed H_2O_2 production procedure depending on the reduction amounts of $^{\cdot}O_2^-$ can be described in the equations below.

$$\text{N-doped } Cu_2O\text{@CuO} + h\nu \rightarrow e^- + h^+ \quad (1)$$

$$O_2 + e^- \rightarrow {}^{\cdot}O_2^- \quad (2)$$

$$^{\cdot}O_2^- + e^- + 2H^+ \rightarrow H_2O_2 \quad (3)$$

It is worthy to point out that the doped N might also serve as an active site for photocatalytic reaction, which might not change the surface distribution, but improve the photochemical stability of Cu_2O-based catalysts and especially the electron transfer ability towards the enhanced photocatalysis performances of the developed N-doped Cu_2O@CuO photocatalysts.

4. Conclusions

In summary, an efficient photocatalyst with N-doped Cu_2O@CuO heterostructure was successfully constructed simply by the one-step N_2 plasma treatment for Cu_2O octahedrons towards the simultaneous N doping and Cu_2O oxidation. The so created heterostructure of N-doped Cu_2O@CuO could present the enhanced photocatalytic activities depending on the plasma treatment time. The highest photocatalytic H_2O_2 production could be achieved for the N-doped Cu_2O@CuO fabricated by 10-min plasma treatment, showing a H_2O_2 production of 12.6 μM after 60 min of visible light irradiation. Also, it can allow for the efficient photocatalytic H_2O_2 production without the need for any precious metal or organic scavengers. Herein, the dramatically enhanced activity of the photocatalytic heterostructure for H_2O_2 production is thought to mainly attributed to the two facts. On the one hand, the CuO derived on the surface of Cu_2O by the in-situ oxidization of N_2 plasma might serve as a new active site for enriching more photogenerated electrons. On the other hand, the doped N might improve the charge separation ability of Cu_2O to facilitate the further increased photogenerated electrons. What's more, the photocatalytic reaction pathway of N-doped Cu_2O@CuO photocatalysts was experimentally demonstrated to feature a two-step single-electron indirect reduction route ($O_2 \rightarrow {}^{\cdot}O_2^- \rightarrow H_2O_2$). This study may provide a simple, rapid, and controllable plasma treatment route for the simultaneous N doping and Cu_2O oxidation of the photocatalysts with enhanced photocatalytic performances. Although the detailed mechanism for the enhancement of photocatalytic H_2O_2 production, this controllable heterostructure construction strategy may be extended for the large-scale design of different kinds of visible-light-driven photocatalysts with the increased

utilization of solar energy and conversion efficiencies for efficient photocatalysis. Therefore, it may promise the wide applications in the photocatalytic energy, environmental protection, and biomedical therapy fields.

CRediT authorship contribution statement

Wenwen Zhang: Data curation, Formal analysis, Investigation, Writing - original draft. **Xi Chen:** Methodology, Software, Writing - original draft. **Xiaoting Zhao:** Software, Validation. **Mengyuan Yin:** Investigation, Resources. **Luping Feng:** Formal analysis, Methodology. **Hua Wang:** Funding acquisition, Project administration, Supervision, Writing - review & editing.

Declaration of Competing Interest

The authors declare that they have no known competing financial interests or personal relationships that could have appeared to influence the work reported in this paper.

Acknowledgements

This work is supported by the National Natural Science Foundations of China (No. 21675099); Major Basic Research Program of Natural Science Foundation of Shandong Province (ZR2018ZC0129), and Key R &D Plan of Jining City (2018HMNS001), Shandong province, P.R. China.

References

[1] L.H. Zheng, H.R. Su, J.Z. Zhang, L.S. Walekara, H.V. Molamahmood, B.X. Zhou, M.C. Long, Y.H. Hu, Highly selective photocatalytic production of H_2O_2 on sulfur and nitrogen co-doped graphene quantum dots tuned TiO_2, Appl. Catal. B: Environ. 239 (2018) 475–484.
[2] J.M. Campos-Martin, G. Blanco-Brieva, J.L.G. Fierro, Hydrogen peroxide synthesis: an outlook beyond the anthraquinone process, Angew. Chem. Int. Ed. 45 (2006) 6962–6984.
[3] A. Asghar, A.A.A. Raman, W.M.A.W. Daud, Advanced oxidation processes for in-situ production of hydrogen peroxide/hydroxyl radical for textile wastewater treatment: a review, J. Clean. Prod. 87 (2015) 826–838.
[4] P. Landon, P.J. Collier, A.J. Papworth, C.J. Kiely, G.J. Hutchings, Direct formation of hydrogen peroxide from H_2/O_2 using a gold catalyst, Chem. Commun. (2002) 2058–2059.
[5] R. Dittmeyer, J.-D. Grunwaldt, A. Pashkovac, A review of catalyst performance and novel reaction engineering concepts in direct synthesis of hydrogen peroxide, Catal. Today 248 (2014) 149–159.
[6] T. Fellinger, F. Hasche, P. Strasser, M. Antoniett, Mesoporous nitrogen-doped carbon for the electrocatalytic synthesis of hydrogen peroxide, J. Am. Chem. Soc. 134 (2012) 4072–4075.
[7] J.Y. Lei, B. Chen, W.J. Lv, L. Zhou, L.Z. Wang, Y.D. Liu, Robust photocatalytic H_2O_2 production over inverse opal g–C_3N_4 with carbon vacancy under visible light, ACS Sustain. Chem. Eng. 7 (2019) 16467–16473.
[8] S.N. Li, G.H. Dong, R. Hailili, L.P. Yang, Y. Li, F. Wang, Y.B. Zeng, C.Y. Wang, Effective photocatalytic H_2O_2 production under visible light irradiation at g-C_3N_4 modulated by carbon vacancies, Appl. Catal. B Environ. 190 (2016) 26–35.
[9] C. Kormann, D.W. Bahnemann, M.R. Hoffmann, Photocatalytic production of H_2O_2 and organic peroxides in aqueous suspensions of TiO_2, ZnO, and desert sand, Environ. Sel. Technol. 22 (1988) 798–806.
[10] G. Moon, W. Kim, A.D. Bokare, N. Sung, W. Choi, Solar production of H_2O_2 on reduced graphene oxide–TiO_2 hybrid photocatalysts consisting of earth-abundant elements only, Energy Environ. Sci. 7 (2014) 4023–4028.
[11] Y. Shiraishi, S. Kanazawa, Y. Kofuji, H. Sakamoto, S. Ichikawa, S. Tanaka, T. Hirai, Sunlight-driven hydrogen peroxide production from water and molecular oxygen by metal-free photocatalysts, Angew. Chem. Int. Ed. 53 (2014) 13454–13459.
[12] Y.M. Yue, P.X. Zhang, W. Wang, Y.C. Cai, F.T. Tan, X.Y. Wang, X.L. Qiao, P.K. Wong, Enhanced dark adsorption and visible-light-driven photocatalytic properties of narrower-band-gap Cu_2S decorated Cu_2O nanocomposites for efficient removal of organic pollutants, J. Hazard. Mater. 384 (2020) 121302.
[13] J.N. Gao, Q.S. Li, H.B. Zhao, L.S. Li, C.L. Liu, Q.H. Gong, L.M. Qi, One-Pot synthesis of uniform Cu_2O and CuS hollow spheres and their optical limiting properties, Chem. Mater. 20 (2008) 6263–6269.
[14] M. Xu, X.H. Liu, W.D. Xu, H.Y. Xu, X.T. Hao, X.J. Feng, Low resistivity phase-pure n-type Cu_2O films realized via post deposition nitrogen plasma treatment, J. Alloy. Compd. 769 (2018) 484–489.
[15] Y. Wang, J. Ghanbaja, F. Soldera, P. Boulet, D. Horwat, F. Mucklich, J.F. Pierson, Controlling the preferred orientation in sputter-deposited Cu_2O thin films: influence of the initial growth stage and homoepitaxial growth mechanism, Acta Mater. 76 (2014) 207–212.
[16] M. Hara, T. Kondo, M. Komoda, S. Ikeda, K. Shinohara, A. Tanaka, J.N. Kondoa, K. Dome, Cu_2O as a photocatalyst for overall water splitting under visible light irradiation, Chem. Commun. (1998) 357–358.
[17] K. Sharma, K. Maiti, N.H. Kim, D. Hui, J.H. Lee, Green synthesis of glucose-reduced graphene oxide supported Ag-Cu_2O nanocomposites for the enhanced visible-light photocatalytic activity, Compos. Part B 138 (2018) 35–44.
[18] Z.H. Wang, S.P. Zhao, S.Y. Zhu, Y.L. Sun, M. Fang, Photocatalytic synthesis of M/Cu_2O (M = Ag, Au) heterogeneous nanocrystals and their photocatalytic properties, CrystEngComm 13 (2011) 2262–2267.
[19] L.M. Liu, W.Y. Yang, W.Z. Sun, Q. Li, J.K. Shang, Creation of Cu_2O@TiO_2 composite photocatalysts with p−n heterojunctions formed on exposed Cu_2O facets, their energy band alignment study, and their enhanced photocatalytic activity under illumination with visible light, ACS Appl. Mater. Inter. 7 (2015) 1465–1476.
[20] M.M. Li, X.F. Xing, Z.Z. Ma, J. Lv, P.C. Fu, Z.X. Li, Synthesis of composition tunable and (111)-faceted Cu/Cu_2O nanoparticles toward photocatalytic, ligand-free, and solvent-free C−N ullmann coupling reactions, ACS Sustain. Chem. Eng. 6 (2018) 5495–5503.
[21] C.J. Munro, E.C. Bell, M.O. Olagunju, J.L. Cohn, E.M. Zahran, L.G. Bachas, M.R. Knecht, Amino acids for the sustainable production of Cu_2O materials: effects on morphology and photocatalytic reactivity, ACS Sustain. Chem. Eng. 7 (2019) 17055–17064.
[22] A.A. Dubale, I.N. Ahmed, X.H. Chen, C. Ding, G.H. Hou, R.F. Guan, X.M. Meng, X.L. Yang, M.H. Xie, A Highly stable metal–organic framework derived phosphorus doped carbon/Cu_2O structure for efficient photocatalytic phenol degradation and hydrogen production, J. Mater. Chem. A 7 (2019) 6062–6079.
[23] A.B. Patil, K.R. Patil, S.K. Pardeshi, Ecofriendly synthesis and solar photocatalytic activity of S-doped ZnO, J. Hazard. Mater. 183 (2010) 315–323.
[24] Y. Matsumoto, M. Koinuma, Y. Iwanaga, T. Sato, S. Ida, N doping of oxide nanosheets, J. Am. Chem. Soc. 131 (2009) 6644–6645.
[25] C. Theerakarunwong, Z.F. Ma, S. Phanichphant, Pt/C doped TiO_2/SWNTs as catalyst for methanol oxidation, J. Nanosci. Nanotechnol. 12 (2012) 3970–3973.
[26] D.H. Jiang, J.B. Xue, L.Q. Wu, W. Zhou, Y.G. Zhang, X.H. Li, Photocatalytic performance enhancement of CuO/Cu_2O heterostructures for photodegradation of organic dyes: effects of CuO morphology, Appl. Catal. B: Environ. 211 (2017) 199–204.
[27] L.M. Liu, W.Y. Yang, Q. Li, S.A. Gao, J.K. Shang, Synthesis of Cu_2O nanospheres decorated with TiO_2 nanoislands, their enhanced photoactivity and stability under visible light illumination, and their post-illumination catalytic memory, ACS Appl. Mater. Interfaces 6 (2014) 5629–5639.
[28] C. Kim, K.M. Cho, A. Al-Saggaf, I. Gereige, H. Jung, Z–scheme photocatalytic CO_2 conversion on three-dimensional $BiVO_4$/carbon-coated Cu_2O nanowire arrays under visible light, ACS Catal. 8 (2018) 4170–4177.
[29] Y.Q. Zhang, B. Ouyang, J. Xu, G.C. Jia, S. Chen, R.S. Rawat, H.J. Fan, Rapid synthesis of cobalt nitride nanowires: highly efficient and low-cost catalysts for oxygen evolution, Angew. Chem. Int. Ed. 55 (2016) 8670–8674.
[30] Y.Y. Wang, C. Xie, Z.Y. Zhang, D.D. Liu, R. Chen, S.Y. Wang, In situ exfoliated, N-Doped, and edge-rich ultrathin layered double hydroxides nanosheets for oxygen evolution reaction, Adv. Funct. Mater. 28 (2018) 1703363.
[31] L. Xu, Q.Q. Jiang, Z.H. Xiao, X.Y. Li, J. Huo, S.Y. Wang, L.M. Dai, Plasma-engraved Co_3O_4 nanosheets with oxygen vacancies and high surface area for the oxygen evolution reaction, Angew. Chem. Int. Ed. 55 (2016) 5277–5281.
[32] A.L. Lamus, G.L. Kok, S.N. Gitlin, J.A. Lind, Automated fluorometric method for hydrogen peroxide in atmospheric precipitation, Anal. Chem. 57 (1985) 917–922.
[33] X.G. Han, X.X. He, L.M. Sun, X. Han, W.W. Zhan, J.H. Xu, X.J. Wang, J.Q. Chen, Increasing effectiveness of photogenerated carriers by in situ anchoring of Cu_2O nanoparticles on a nitrogen-doped porous carbon Yolk−Shell cuboctahedral framework, ACS Catal. 8 (2018) 3348–3356.
[34] X. Han, X.X. He, F. Wang, J.Q. Chen, J.H. Xu, X.J. Wang, X.G. Han, Engineering an N-doped Cu_2O@N–C interface with long-lived photo-generated carriers for efficient photoredox catalysts, J. Mater. Chem. A 5 (2017) 10220–10226.
[35] S. Shenawi-Khalil, V. Uvarov, S. Fronton, I. Popov, Y. Sasson, A Novel Heterojunction BiOBr/bismuth oxyhydrate photocatalyst with highly enhanced visible light photocatalytic properties, J. Phys. Chem. C 116 (2012) 11004–11012.
[36] J.L. Pan, W.Q. Liu, L. Quan, N. Han, S.L. Bai, R.X. Luo, Y.J. Feng, D.Q. Li, A.F. Chen, Cu_2O and rGO hybridizing for enhancement of low-concentration NO_2 sensing at room temperature, Ind. Eng. Chem. Res. 57 (2018) 10086–10094.
[37] X.R. Zhang, Y.H. Lin, J.F. Zhang, D.Q. He, D.J. Wang, Photoinduced charge carrier properties and photocatalytic Activity of N-doped TiO_2 nanocatalysts, Acta Phys. Chim. Sin. 26 (2010) 2733–2738.
[38] W. Ong, L. Tan, Y.H. Ng, S. Yong, S. Chai, Graphitic carbon nitride (g-C_3N_4)-based photocatalysts for artificial photosynthesis and environmental remediation: are we a step closer to achieving sustainability? Chem. Rev. 116 (2016) 7159–7329.
[39] G.M. Ba, Z.W. Liang, H.P. Li, N. Du, J.Q. Liu, W.G. Hou, Simultaneous formation of mesopores and homojunctions in graphite carbon nitride with enhanced optical absorption, charge separation and photocatalytic hydrogen evolution, Appl. Catal. B Environ. 253 (2019) 359–368.
[40] X.M. Gao, Y.Y. Shang, L.B. Liu, F. Fu, Chemisorption-enhanced photocatalytic nitrogen fixation via 2D ultrathin p–n heterojunction AgCl/d-Bi_2O_3 nanosheets, J. Catal. 371 (2019) 71–80.
[41] H.Y. Li, Y.J. Sun, B. Cai, S.Y. Gan, D.X. Han, L. Niu, T.S. Wu, Hierarchically Z-scheme photocatalyst of Ag@AgCl decorated on $BiVO_4$ (040) with enhancing photoelectrochemical and photocatalytic performance, Appl. Catal. B Environ. 170 (2015) 206–214.
[42] K.P.S. Parmar, H.J. Kang, A. Bist, P. Dua, J.S. Jang, J.S. Lee, Photocatalytic and photoelectrochemical water oxidation over metal-doped monoclinic $BiVO_4$ photoanodes, ChemSusChem 5 (2012) 1926–1934.
[43] T. Baran, S. Wojtyła, A. Minguzzi, S. Rondinini, A. Vertova, Achieving efficient H_2O_2 production by a visible-light absorbing, highly stable photosensitized TiO_2, Appl. Catal. B Environ. 244 (2019) 303–312.
[44] W.C. Hou, Y.S. Wang, Photocatalytic generation of H_2O_2 by graphene oxide in organic electron donor-free condition under sunlight, ACS Sustain. Chem. Eng. 5 (2017) 2994–3001.